Mon. Not. R. astr. Soc., (1986) **218**, 331–361

Studies of broad emission line profiles in QSOs – II. Properties of a large, predominantly radio selected sample

Belinda J. Wilkes★ *Steward Observatory, University of Arizona, Tucson, AZ 85721, USA*

Accepted 1985 August 13. Received 1985 June 17; in original form 1984 April 5

Summary. Emission line parameters for 214 QSOs are reported. The majority were originally selected according to the flatness of their radio spectra from the Parkes 2700, 5000 MHz surveys. The optical spectra of these objects were presented graphically in an earlier paper (WWJP, see text). Preliminary studies of the properties of this sample, including line velocity width and equivalent width distributions, have been made. Specific emission lines have been investigated in more detail to confirm or refute earlier results.

1 Introduction

The basic physical conditions of the radiating gas in the broad emission line region (BELR) of QSOs are well established (see e.g. Davidson & Netzer 1979; Kwan & Krolik 1981); only the finer details remain to be debated. This is not the case, however, for the spatial distribution or dynamics of the gas, for which there remain a large number of competing models (Blumenthal & Mathews 1975, 1979; Mathews 1974; Kwan & Carroll 1982; Krolik & London 1983). The common denominator of these models is generally a large number of small, optically thick clouds or filaments providing a low covering factor and moving at high velocities; the sense of this motion has not been determined. The main reason for the lack of a more specific model is the shortage of observational constraints. The stellar nature of QSOs prohibits any direct observation of the gas motion and, although a composite picture is provided by the shapes of the emission line profiles, their study is difficult for the following reasons. First, QSOs are faint and it is both time-consuming and laborious to obtain the necessary high-quality data; secondly, the properties of QSO spectra are diverse and there can be no certainty that the few bright ones that are studied in detail are representative of QSOs as a whole. It is therefore necessary to approach the problem in two different ways: first to study the line profiles of a small number of QSOs in detail (Wilkes 1984; Paper I hereafter); secondly to investigate the distribution of first-order properties over a larger sample both for their own sake, to shed some light on the class as a whole, and also to facilitate comparison with the smaller sample to determine how typical the latter objects are.

In a recent publication (Wilkes *et al.* 1983, WWJP hereafter) the optical spectra of 295 QSO

★ Present address: Smithsonian Astrophysical Observatory, 60 Garden Street, Cambridge, MA 02138, USA.

candidates are presented; the majority of these were originally selected from the Parkes 2700 and 5000 MHz radio surveys by their flat spectral index ($\alpha<0.5$). In this paper emission line measurements are presented for those active galactic nuclei (AGNs) in the sample which possess measurable lines. A very important attribute of this sample is the fact of radio selection which results in its being relatively unbiased in terms of optical properties, in particular, the strengths and widths of the emission lines, upon which objective prism surveys (for example) are heavily dependent. Consequently, although it is not a well-defined sample in the sense of being complete to a specific flux level, it is randomly selected in terms of its optical emission line properties. It is therefore a good starting point for a study of the range of these properties present in AGNs. Similar studies for steep spectrum radio sources have been made (e.g. Baldwin *et al.* 1973; Smith *et al.* 1977, and references therein). The quality of the spectral data in both resolution and signal-to-noise (S/N) properties varies widely from object to object and thus the sample is incomplete at low equivalent widths. It should be noted that a number of the AGNs in the WWJP compilation are optically selected and are included in this paper for completeness. They are not free from bias in terms of optical properties and were not included in full sample analysis unless otherwise noted.

Throughout this paper each object is referred to by PKS coordinate designation. A number of the objects have been studied by other authors on the basis of different data and are also known by other names. Such information can be found by referring to one of the QSO catalogues (Hewitt & Burbidge 1980; Véron-Cetty & Véron 1984) and will not be repeated here except in a small number of cases. All measurements reported here are based on these data alone; confirmatory or conflicting results from the literature are noted where relevant. No attempt has been made to distinguish between SyI galaxies and QSOs on the basis of these data.

2 Observations

The optical spectra for this sample were obtained using the 4-m Anglo–Australian Telescope (AAT), the RGO spectrograph and associated Image Dissector Scanner (IDS) and/or Image Photon Counting System (IPCS) detectors by a number of observers during the period 1975–80 (WWJP, Jauncey *et al.* 1984, and references therein). References are given in Table 1 to the original papers discussing the present data, and observational details for individual QSOs may be found there. As described in WWJP, many of the objects were observed several times during this period and the data summed to improve the S/N provided no variability was detected. No strong constraints on variability exist, however, due to the low S/N of the spectral data and lack of photometry. The measurements presented here represent a mean over a time-scale of a few years between 1975 and 1980. Graphical presentation of the optical spectra, details of observed wavelength range, photometric quality, resolution, etc. may be found in WWJP. In this paper spectral line positions, identifications, widths, equivalent widths and intensity ratios are reported. The distribution of these properties for each line was studied; general results, along with a more detailed discussion of several of the broad lines, are given below.

3 Measurement

Measurement of emission line parameters, such as full-width-half-maximum (FWHM) and flux, are subjective, particularly for low-quality data. It is advantageous when studying a large number of objects for all measurements to be made in a consistent manner; consequently, all the spectra were measured, including those that have been studied previously (see references in Table 1). Measurement errors are present due to weak, blended emission and absorption features as well as noise; these are best judged by inspecting the individual profiles in WWJP.

Table 1

Object	Redshift	Ref.	Line	Peak Wavelength Å	FWHM kms-1	W Å	Relative Flux	Notes
0002-422*	2.758		OVI λ1034	3891	3130	19	23	OS
			HI λ1216	4571	5450	320	338	SB, BW
			NV λ1240	4680	4600	143	155	
			OI λ1304	4919	1220	14	16	
			OIV]/SiIV λ1400	5281	2650	9	11	
			CIV λ1549	5818	5410	92	100	
			HeII λ1640	6170	400	--	1	Weak
			CIII] λ1909	7163	6480	48	39	Noisy
0005-239	1.412	2,10	CIV λ1549	3742	6260	61	100	Noisy
			CIII] λ1909	4597	3620	26	32	
			MgII λ2798	6752	3200	19	15	
0007+106 (III Zw2)	0.090		[OII] λ3727	4063	960	1	2	
			[NeIII] λ3869	4215	1210	4	9	
			HI λ4102	4461	2840	4	6	
			HI λ4340	4738	4410	18	30	
			HI λ4861	5298	5230	76	100	
			[OIII] λ4959	5405	670	6	8	
			[OIII] λ5007	5456	600	21	26	
0008-264*	1.093		CIII] λ1909	3984	4790	141	---	MgII ~ 5860
0029-414*	0.891	3	CIII] λ1909	3599	9349	152	320	
			MgII λ2798	5308	7456	100	100	
0036-392*	0.592	1	MgII λ2798	4449	5080	51	100	
			[NeV] λ3426	5461	550	3	4	
			[OII] λ3727	5943	1390	20	23	
0044+030	0.621	1	MgII λ2798	4539	6080	51	100	
			[OII] λ3727	6040	2900	9	12	
0046-315*	2.719	1	HI λ1216	4515	3540	120	720	SB, BW
			NV λ1240	4614	2430	36	220	
			OIV]/SiIV λ1400	5183	2620	6	34	
			CIV λ1549	5756	2400	20	100	
			CIII] λ1909	7112	2800	25	97	At end of scan
0047-832	1.114	3	CIII] λ1909	4033	3520	47	186	
			MgII λ2798	5919	3370	28	100	
0047-579	1.792	1	OIV]/SiIV λ1400	3900	3000	12	13	
			CIV λ1549	4325	4000	112	100	
			CIII] λ1909	5330	5800	23	16	
0048-071*	1.974	10	HI λ1216	3619	7720	224	124	SB
			NV λ1240	----	----	31	17	
			OIV]/SiIV λ1400	4188	6050	28	14	
			CIV λ1549	4615	5960	328	100	
			HeII λ1640	4890	----	152	55	Blended FeII
			CIII] λ1909	5651	9200	135	45	
0049-393*	2.831		OVI λ1034	3938	8100	160	82	OS
			HI λ1216	4665	4630	272	180	SB
			NV λ1240	4741	4995	136	90	
			SiII λ1264	4869	4995	54	35	
			OI λ1304	5028	----	---	---	
			OIV]/SiIV λ1400	5409	2700	11	7	
			CIV λ1549	5941	7760	169	100	
			HeII λ1640	6396	4780	41	21	
0054-006*	2.777	1	HI λ1216	4595	9990	166	280	SB
			NV λ1240	----	----	41	70	
			SiII λ1264	----	----	32	53	
			OIV]/SiIV λ1400	5260	2800	10	15	
			CIV λ1549	5842	8640	73	100	

Table 1 – *continued*

Object	Redshift	Ref.	Line	Peak Wavelength Å	FWHM kms-1	W Å$^{\lambda}$	Relative Flux	Notes
0100-270	1.600	3	CIV λ1549	4019	4770	64	100	
			HeII λ1640	4265	1410	5	7	
			CIII] λ1909	4959	4470	32	28	
0101-76	1.015	3	MgII λ2798	5637	4760	38	---	1 line
0108-079	1.773	10	HI λ1216	3376	5700	340	330	SB, BW
			NV λ1240	3453	1310	50	65	
			SiII λ1264	3515	2480	35	47	
			OI λ1304	3645	2800	---	2	
			CII λ1335	3784	1950	4	5	ID?
			OIV]/SiIV λ1400	3909	2500	17	7	
			CIV λ1549	4303	3600	141	100	
			HeII λ1640	4567	6400	---	44	blended FeII
			CIII] λ1909	5281	8160	45	35	
0113-118	0.672	10	MgII λ2798	4678	4620	83	---	1 line
0116-219	1.161	10	CIV λ1549	3334	8160	65	100	
			CIII] λ1909	4140	8330	45	40	
			MgII λ2798	6052	3080	28	22	At end of scan
0122-042	0.561		MgII λ2798	4361	3920	49	---	
			[NeV] λ3426	5355	----	---	---	Weak
0125-414	1.099		MgII λ2798	5874	1890	25	---	1 line
0130-17	1.022	10	CIII] λ1909	3860	----	---	---	
			MgII λ2798	5654	2440	48	---	
0133-203	1.141	10	CIV λ1549	3316	6020	128	100	
			CIII] λ1909	4082	6310	70	28	
			MgII λ2798	6002	6760	76	26	
0135-247	0.829	3,10	CIII] λ1909	3477	6960	94	260	
			MgII λ2798	5139	4220	80	100	
0136-231	1.893		HI λ1216	3508	4860	386	250	RC
			NV λ1240	3583	1590			
			OIV]/SiIV λ1400	4053	5800	15	9	
			CIV λ1549	4492	5680	169	100	
			CIII] λ1909	5524	4220	27	13	
0142-278	1.153	10	CIV λ1549	3332	----	---	---	At end of scan
			CIII] λ1909	4101	8760	52	106	
			MgII λ2798	6042	5780	72	100	
0146-500	2.261	11	HI λ1216	3960	3850	300	760	SB, BW
			NV λ1240	4050	4150	90	230	
			SiII λ1264	----	----	27	68	
			OI λ1304	4256	3250	7	16	
			CIV λ1549	5055	4300	78	100	
			CIII] λ1909	6231	2600	58	45	
0150-334*	0.610	2	MgII λ2798	4509	4600	52	100	
			[NeV] λ3426	5558	6255	35	50	Redshifted, ID?
			[OII] λ3727	5996	3300	16	20	
0158-490	0.310	11	HeII λ3220	4215	430	2	8	OS
			[NeIII] λ3869	5076	5270	7	18	
			HI λ4102	5396	4410	11	26	
			HI λ4340	5671	3770	24	54	
			HI λ4861	6359	----	43	100	
			[OIII] λ4959					
			[OIII] λ5007	6550	780	5	10	
0202-76	0.391	3	MgII λ2798	3881	7900	85	430	
			[OII] λ3727	5180	640	5	13	
			HI λ4340	6054	2580	19	30	
			HI λ4861	6791	7320	77	100	
			[OIII] λ4959	6891	650	13	21	
			[OIII] λ5007	6955	990	99	140	

Table 1 – *continued*

Object	Redshift	Ref.	Line	Peak Wavelength Å	FWHM kms-1	W Å$^{\lambda}$	Relative Flux	Notes
0208-512	1.003	1	CIII] λ1909	3815	2080	12	95	
			MgII λ2798	5615	4070	18	100	
0213-484	0.168	11	[NeV] λ3426	3991	2920	10	35	OS
			HI λ4340	5070	1480	10	26	
			HI λ4861	5678	2870	42	100	
			[OIII] λ4959	5795	1190	7	16	
			[OIII] λ5007	5851	1130	21	49	
0219-164	0.7		MgII λ2798	4756	2300	59	---	1 line
0222-00 (4C00.12)	0.683	2	MgII λ2798	4701	----	---	---	
			[OII] λ3727	6275	1460	15	100	
			[NeIII] λ3869	6513	2240	14	85	
			[NeIII] λ3968	6681	2160	10	60	
0222+000	0.525	1	MgII λ2798	4265	6470	70	100	
			HeII λ3220	4916	2140	6	8	
			[NeV] λ3426	5215	1680	13	13	
			[OII] λ3727	5685	1950	9	8	
0234-301*	2.101	1	HI λ1216	3772	5880	204	420	SB
			NV λ1240	3856	3120	105	150	
			OI λ1304	4060	4080	12	20	
			CII λ1335	4180	4200	8	12	
			OIV]/SiIV λ1400	4341	6010	24	35	
			CIV λ1549	4790	5560	86	100	
0237-23 (PHL8462)	2.220		HI λ1216	3917	6590	189	330	SB, BW
			NV λ1240	3970	7510	66	120	
			SiII λ1264	4049	----	---	---	
			OI λ1304	4211	2570	5	8	
			CII λ1335	4317	3840	5	8	
			OIV]/SiIV λ1400	4518	4430	9	13	
			CIV λ1549	4981	7200	92	100	
0252-549	0.541	3	MgII λ2798	4296	7380	92	100	
			[NeV] λ3426	5261	1320	5	3	
			[NeIII] λ3869	5977	1230	5	3	
			[NeIII] λ3968	6108	1110	4	2	
0253-218	1.470		CIV λ1549	3831	4120	87	100	
			CIII] λ1909	4710	7800	57	28	
0254-334/R*	1.906	1,15	HI λ1216	3537	4670	352	270	NV weak
			OI λ1304	3786	----	---	---	
			CIV λ1549	4498	4330	131	100	
			HeII λ1640	4763	1380	3	2	
0254-334/2*	1.863	1,13 15	HI λ1216 / NV λ1240	3544	3310	70	220	Profiles redward of broad absorption trough
			CII λ1335	3855	----	---	---	
			OIV]/SiIV λ1400	4013	1520	8	20	
			CIV λ1549	4433	4120	50	100	
			CIII] λ1909	5460	6900	61	80	
0312-77	0.224	3	HeII λ3220	3919	760	5	10	
			[OII] λ3727	4563	660	2	4	
			[NeIII] λ3869	4733	1080	2	3	
			HI λ4102	5022	2540	8	9	
			HI λ4340	5321	2990	21	26	
			HI λ4861	5954	3230	90	100	
			[OIII] λ4959	6073	640	8	9	
			[OIII] λ5007	6133	690	37	38	
0329-255*	2.690	3	HI λ1216	4464	7160	144	240	SB, BW
			NV λ1240	4550	4500	83	140	
			SiII λ1264	----	----	6	10	
			OIV]/SiIV λ1400	5161	3480	14	20	
			CIV λ1549	5709	6900	88	100	

Table 1 – *continued*

Object	Redshift	Ref.	Line	Peak Wavelength Å	FWHM kms-1	W Å$^{\lambda}$	Relative Flux	Notes
0347-241	1.885		HI λ1216	3509	8810	252	480	SB
			NV λ1240	3581	2420	43	82	Uncertain
			SiII λ1264	----	----	10	20	
			CIV λ1549	4467	11800	60	100	
0355-079	1.050		CIII] λ1909	3912	4030	17	---	
			MgII λ2798	5736	3890	53	---	Strong cental absorption
0355-483	0.997	2,16	CIII] λ1909	3790	----	---	---	Weak + uncertain
			MgII λ2798	5606	5450	29	---	
0402-362	1.421	1	CIV λ1549	3766	6240	44	100	
			CIII] λ1909	4606	4540	15	26	
0406-127	1.568	5,10	OIV]/SiIV λ1400	3598	2000	22	38	
			CIV λ1549	3965	5100	62	100	
			CIII] λ1909	4917	5730	39	50	
0413-21	0.808	10	CIII] λ1909	3414	5950	38	75	
			CII] λ2326	4202	4500	11	15	
			MgII λ2798	5061	2670	64	100	
0414-189*	1.522	5,10	CIV λ1549	3908	4400	38	---	
0422-380	0.782	2	MgII λ2798	4990	4420	17	100	
			[NeV] λ3426	6104	3420	7	34	
0434-188	2.705	10	OIV λ1034	3827	3300	22	32	
			HI λ1216	4506	2500	239	450	
			NV λ1240	4589	3960	117	140	
			SiII λ1264	----	----	23	27	
			OIV]/SiIV λ1400	5187	4100	26	32	
			CIV λ1549	5741	3190	79	100	
0435-300	1.324	5	CIV λ1549	3599	4290	47	100	
			CIII] λ1909	4440	3380	18	28	
			MgII λ2798	6515	----	---	---	
0436-129	1.277		CIV λ1549	3528	4300	159	100	
			CIII] λ1909	4347	6940	40	19	
0439-433	0.593		MgII λ2798	4453	4000	43	100	
			HI λ4102	6525	2360	6	6	
			HI λ4340	6951	3400	19	18	
0448-392	1.291	2	CIV λ1549	3551	4800	57	100	
			CIII] λ1909	4368	4500	54	50	
			MgII λ2798	6418	2840	30	22	
0448-187*	2.05		CIV λ1549	4725	4730	38	---	1 line
0451-28	2.559	10	OVI λ1034	3658	11680	50	60	
			HI λ1216	4330	3700	264	270	BW
			NV λ1240	4397	3640	132	140	
			SiII λ1264	----	----	26	27	
			OI λ1304	4642	2880	16	17	
			CII λ1335	4742	1230	5	5	
			OIV]/SiIV λ1400	4961	4600	17	18	
			CIV λ1549	5508	4970	95	100	
0454-22	0.532	5	MgII λ2798	4286	4480	51	---	1 line
0454+039	1.346	2	CIV λ1549	3627	5740	69	100	
			NIII] λ1750	4117	----	---	---	
			CIII] λ1909	4466	3220	16	23	
			MgII λ2798	6576	4020	36	39	
0506-61	1.087	2	CIII] λ1909	3980	6550	31	120	
			MgII λ2798	5846	3270	45	100	

Table 1 – *continued*

Object	Redshift	Ref.	Line	Peak Wavelength Å	FWHM kms-1	W Å$^{\lambda}$	Relative Flux	Notes
0514-161	1.275	2	CIII] λ1909	4336	3300	33	65	
			MgII λ2798	6377	5560	71	100	
0522-611	1.389	5	CIV λ1549	3695	----	57	100	
			CIII] λ1909	4567	9470	44	40	
0537-441*	0.893	1	MgII λ2798	5297	3200	19	---	
0537-286*	3.119	5,6	HI λ1216 / NV λ1240	5016	----	176	140	
			OIV]/SiIV λ1400	5770	3020	15	10	
			CIV λ1549	6371	12130	163	100	
0602-319	0.450	2,15	MgII λ2798	4040	2770	10	19	Unusually weak
			[OII] λ3727	5404	2340	13	23	
			[NeIII] λ3869	5608	2780	10	17	
			[NeIII] λ3968	5765	2530	7	12	
			HI λ4340	6305	7580	16	28	
			HI λ4861	7097	8500	---	---	Very broad
			[OIII] λ4959	7198	750	7	14	
			[OIII] λ5007	7263	1980	53	100	
0606-223	1.928	5	HI λ1216 / NV λ1240	3557	4070	359	210	
			CIV λ1549	4537	3080	164	100	
0621-786	0.942	3	MgII λ2798	5433	3150	30	---	1 line
0622-441	0.680	2	MgII λ2798	4700	5000	50	---	
0637-752	0.656	16	MgII λ2798	4636	4730	64	100	
			[NeIII] λ3869	6398	1030	6	5	
			HI λ4102	6788	----	---	---	
			HI λ4340	7192	4800	27	21	
0642-349	2.162	2	HI λ1216	3839	3240	152	260	SB, BW
			NV λ1240	3934	3560	22	36	
			OI λ1304	4137	1460	3	---	
			CIV λ1549	4899	3030	62	100	
			HeII λ1640	5183	2370	11	18	
			CIII] λ1909	6047	6740	38	54	
0723-008*	0.129	2	[OII] λ3727	4200	5670	30	107	N galaxy
			HI λ4861	5494	----	---	---	
			[OIII] λ4959	5598	1180	6	28	
			[OIII] λ5007	5652	3380	22	100	
0748+126*	0.884	4	MgII λ2798	5273	2750	41	---	
0812+02	0.404		MgII λ2798	3929	4350	68	100	
			[NeV] λ3426	4808	690	3	3	
			[OII] λ3727	5231	920	6	3	
			[NeIII] λ3869	5428	720	4	2	
			HI λ4102	5767	2660	11	4	Noisy
			HI λ4340	6101	4060	40	12	
			HI λ4861	6830	5080	100	28	Noisy
			[OIII] λ4959	6957	860	36	10	
			[OIII] λ5007	7025	600	63	17	
0819-032	2.355	2	HI λ1216	4084	4780	237	330	SB, BW
			NV λ1240	----	----	26	36	
			OI λ1304	4420	----	---	---	
			CII λ1335	4492	----	---	---	
			OIV]/SiIV λ1400	4709	7060	24	27	
			CIV λ1549	5199	2980	101	100	
			HeII λ1640	5501	4250	22	2	
			CIII] λ1909	6392	8850	51	40	
0845-051	1.238	5	CIV λ1549	3475	7140	43	100	
			CIII] λ1909	4260	7760	25	33	

Table 1 – *continued*

Object	Redshift	Ref.	Line	Peak Wavelength Å	FWHM kms-1	W Å$^{\lambda}$	Relative Flux	Notes
0858-77*	0.489		MgII λ2798	4178	5900	33	100	
			[NeV] λ3426	5103	2060	6	22	
			[OII] λ3727	5560	970	4	16	
			[NeIII] λ3869	5755	1200	6	23	
			HI λ4102	6074	3000	18	45	
			HI λ4340	6475	2720	16	42	
			HI λ4861	7215	----	---	---	Very Noisy
			[OIII] λ4959	7397	1300	48	120	
			[OIII] λ5007	7455	1250	91	210	
0859-14	1.333		CIV λ1549	3609	4730	73	100	
			CIII] λ1909	4455	4040	27	23	
			MgII λ2798	6537	4060	26	12	
0902-256	1.640	5	OI λ1304	3474	----	---	---	
			CII λ1335	3556	----	---	---	
			OIV]/SiIV λ1400	3700	3860	15	20	
			CIV λ1549	4095	5450	85	100	
			CIII] λ1909	5030	6630	33	32	
0906+01	1.029	2	CIII] λ1909	3880	6160	27	130	
			MgII λ2798	5671	3990	29	100	
			[NeV] λ3426	6950	1230	4	9	
0915-213	0.849	5	CIII] λ1909	3523	4220	52	120	
			MgII λ2798	5175	2490	59	100	
			[NeV] λ3426	6337	----	---	---	Noisy
0919-260	2.297	5	OVI λ1034	3406	1940	15	35	
			HI λ1216	4016	3370	130	230	SB, BW
			NV λ1240	4082	3960	43	76	
			SiII λ1264	----	----	12	20	
			OIV]/SiIV λ1400	4611	5910	23	34	Noisy
			CIV λ1549	5110	2470	51	100	
			HeII λ1640	5428	1170	6	9	
0925-203	0.347	4	MgII λ2798	3769	3500	47	100	
			[NeIII] λ3869	5213	1270	5	2	
			[NeIII] λ3968	5342	2920	5	4	
			HI λ4102	5528	2360	11	9	
			HI λ4340	5857	3580	29	20	
			HI λ4861	6549	2770	58	39	
			[OIII] λ4959	6681	670	4	2	
			[OIII] λ5007	6746	890	25	15	
0959-443	0.837	2,5	CIII] λ1909	3498	7270	39	85	
			MgII λ2798	5152	7880	42	100	
1004-217	0.331		MgII λ2798	3723	2340	19	100	
			[NeIII] λ3869	5170	----	---	---	
			[NeIII] λ3968	5275	----	---	---	
			HI λ4340	5781	1610	12	26	
			HI λ4861	6469	2430	40	67	
			[OIII] λ5007	6653	----	---	---	
1004+141	2.707	5	HI λ1216	4508	----	---	---	
			OIV]/SiIV λ1400	5154	----	---	---	
			CIV λ1549	5740	----	---	---	
1009-321	1.757	16	CIV λ1549	4269	5200	149	100	
			FeII λ1660	4576	2820	11	6	
			CIII] λ1909	5264	7380	43	21	
			CII] λ2326	6438	6270	28	10	
1032-199	2.189	5	HI λ1216	3879	4640	200	370	RC
			NV λ1240	3953	1430	---	---	
			SiII λ1264	4016	2230	---	---	
			OIV]/SiIV λ1400	4450	----	---	---	
			CIV λ1549	4952	4250	66	100	

Table 1 – *continued*

Object	Redshift	Ref.	Line	Peak Wavelength Å	FWHM kms-1	W Å$^{\lambda}$	Relative Flux	Notes
1101-325	0.356	2	MgII λ2798	3788	3620	43	100	
			[NeV] λ3426	4646	1610	4	13	
			[NeIV] λ3485	4726	2250	4	7	
			[OII] λ3727	5051	1190	3	4	
			[NeIII] λ3869	5245	1740	4	6	
			[NeIII] λ3968	5381	1670	4	5	
			HI λ4102	5562	2050	9	9	
			HI λ4340	5904	3870	41	38	
			HI λ4861	6589	3030	145	139	
			[OIII] λ4959	6717	940	12	16	
			[OIII] λ5007	6783	970	59	69	
1103-006	0.425	2	MgII λ2798	3992	4930	38	100	
			[NeIII] λ3968	5655	1380	3	3	
			HI λ4340	6183	4950	27	26	
			HI λ4861	6950	5460	55	46	
			[OIII] λ4959	7056	----	---	4	
			[OIII] λ5007	7118	840	8	8	
1104-445	1.596	4	CIV λ1549	4024	2980	40	100	
			NIII] λ1750	4545	----	---	---	
			CIII] λ1909	4951	5120	31	47	
1111+149*	0.870	4	MgII λ2798	5225	2380	20	---	
1117-248*	0.465	16	MgII λ2798	4092	6260	20	100	
			[OII] λ3727	5460	770	4	9	
			[NeIII] λ3869	5672	1270	3	6	
			HI λ4861	7130	5560	72	120	
			[OIII] λ4959	7265	870	8	15	
			[OIII] λ5007	7341	1390	36	60	
1127-14	1.184		CIV λ1549	3366	4880	38	100	
			HeII λ1640	3583	----	---	---	
			CIII] λ1909	4172	6190	55	77	
			MgII λ2798	6131	2750	38	28	
1136-13	0.557		MgII λ2798	4358	2690	22	100	
			[NeV] λ3426	5333	960	---	---	
			[OII] λ3727	5800	----	---	---	
			[NeIII] λ3869	6020	700	3	5	
			HI λ4102	6380	800	4	8	
			HI λ4340	6773	2890	26	52	
1145-071	1.342		CIV λ1549	3630	3890	203	100	
			CIII] λ1909	4468	4860	39	12	
1146-037*	0.341	2	MgII λ2798	3752	6240	42	100	
			[NeV] λ3426	4591	1110	3	5	
			[OII] λ3727	4998	1140	6	10	
			[NeIII] λ3869	5188	1620	15	20	
			[NeIII] λ3968	5315	1380	8	9	
			HI λ4340	5831	6470	30	28	
			HI λ4861	6512	4070	130	80	
			[OIII] λ4959	6645	1040	29	32	
			[OIII] λ5007	6708	940	105	104	
1148-171*	1.751	5	HI λ1216	3344	4630	121	260	SB
			NV λ1240	----	----	40	90	Uncertain
			OIV]/SiIV λ1400	3862	5610	24	37	
			CIV λ1549	4259	2600	77	100	
			CIII] λ1909	5252	5280	79	83	
1151-34*	0.257	3	[OII] λ3727	4687	2110	18	24	
			[NeIII] λ3869	4857	1600	6	9	
			HI λ4102	5188	870	3	4	
			HI λ4861	6102	9430	---	---	
			[OIII] λ4959	6236	960	16	39	
			[OIII] λ5007	6300	1100	42	100	

Table 1 – *continued*

Object	Redshift	Ref.	Line	Peak Wavelength Å	FWHM kms-1	W Å$^{\lambda}$	Relative Flux	Notes
1157+014*	1.981	2,12	CIV λ1549	4644	5890	---	---	
			HeII λ1640	4885	3220	9	29	
			CIII] λ1909	5697	7990	33	100	
1157-215	0.931	16	MgII λ2798	5419	3250	43	100	
			HeII λ3220	6218	820	3	6	
			[NeV] λ3426	6604	770	3	6	
1158+007*	1.370	2	CIII] λ1909	4502	7060	37	50	
			MgII λ2798	6649	5720	95	100	
1200-051*	0.379	5	MgII λ2798	3857	2540	18	100	
			[OII] λ3727	5143	820	11	35	
			HI λ4102	5633	740	5	14	
			HI λ4340	5987	1150	24	70	
			HI λ4861	6712	1140	57	140	
			[OIII] λ5007	6910	740	37	85	
1203-26	0.789	5	CIII] λ1909	3415	3950	115	64	
			MgII λ2798	5004	4050	168	100	
1205-008	1.007	2	MgII λ2798	5615	3690	50	---	1 line
1207-399	0.964	3	CIII] λ1909	3746	5520	12	100	
			CII] λ2326	4563	4270	6	15	
			MgII λ2798	5510	3410	32	120	
1215+013*	0.117	2	[OII] λ3727	4165	----	---	---	
			HI λ4861	5428	610	4	21	
			[OIII] λ4959	5540	1190	2	13	
			[OIII] λ5007	5593	1070	8	45	
			HI λ6563	7333	2170	15	100	
1219+04	0.965		MgII λ2798	5498	2780	29	---	1 line
1229-021 (4C02.55)	1.043		CIII] λ1909	3896	5000	46	130	
			MgII λ2798	5727	3490	49	100	
1232-249	0.356	5	MgII λ2798	3801	7250	33	16	
			[NeV] λ3426	4646	1550	7	5	
			[OII] λ3727	5055	1100	14	10	
			[NeIII] λ3869	5247	1290	7	5	
			[NeIII] λ3968	5377	1580	6	3	
			HI λ4102	5554	2510	10	4	
			HI λ4340	5882	2900	43	24	
			HI λ4861	6595	1740	33	22	
			[OIII] λ4959	6727	2270	81	47	
			[OIII] λ5007	6791	1310	175	100	
1240-294	1.130	2,15	CIII] λ1909	4049	10030	58	270	
			MgII λ2798	5982	4780	51	100	
1243-072	1.286	5	CIV λ1549	3535	3470	48	100	
			CIII] λ1909	4353	1580	5	67	
1244-255	0.638	16	MgII λ2798	4586	2720	31	100	
			[OII] λ3727	6077	1770	5	12	
			HI λ4102	6727	1760	5	10	
			HI λ4340	7127	1920	12	24	
1254-333	0.190	3	HI λ4340	5163	6850	24	170	
			HI λ4861	5777	----	97	640	
			[OIII] λ4959					
			[OIII] λ5007	5962	2220	16	100	
1311-270*	2.260		HI λ1216	3968	5050	170	340	SB, BW
			NV λ1240	4054	4750	59	120	
			OIV]/SiIV λ1400	4561	----	---	---	
			CIV λ1549	5035	2660	41	100	

Table 1 – *continued*

Object	Redshift	Ref.	Line	Peak Wavelength Å	FWHM kms-1	W Å$^{\lambda}$	Relative Flux	Notes
1327-214*	0.525		MgII λ2798	4269	3970	58	---	
			[NeV] λ3426	5222	----	---	---	
			[OII] λ3727	5685	----	---	---	
			[NeIII] λ3869	5900	----	---	---	
			HI λ4102	6257	----	---	---	
			HI λ4340	6629	----	---	---	
1327-206	1.169	16	CIII] λ1909	4131	6780	64	57	
			CII] λ2326	5034	4070	5	6	
			MgII λ2798	6076	6100	89	100	
			HeII λ3220	7001	4040	16	16	
1327-311	1.335	4	NIII] λ1750	4090	----	---	---	
			CIII] λ1909	4459	2990	14	72	
			MgII λ2798	6528	3600	25	100	
1335-127	0.541		MgII λ2798	4306	3790	40	---	1 line
1335+023	1.356	4	CIII] λ1909	4495	4040	29	105	
			MgII λ2798	6591	4850	42	100	
1336-000*	1.808		OIV]/SiIV λ1400	3928	----	31	26	
			CIV λ1549	4350	----	146	100	
			CIII] λ1909	5364	9960	---	---	
1352-104	0.330	14	MgII λ2798	3724	3260	49	---	1 line
1354-152	1.89		OIV]/SiIV λ1400	4021	7230	14	23	
			CIV λ1549	4491	6740	67	100	
			CIII] λ1909	5511	7450	46	57	
1355-41*	0.314		MgII λ2798	3674	10720	63	100	
			HeII λ3220	4233	8010	19	33	
			[NeV] λ3426	4541	5030	7	12	
			HI λ4861	6376	----	---	---	
1402+044	3.204	4,7	OVI λ1034	4352	6660	94	33	
			HI λ1216	5112	3920	510	200	BW, RC
			NV λ1240	5223	5270	130	50	
			CIV λ1549	6504	9720	308	100	
1403-085	1.758	5	HI λ1216 / NV λ1240	3346	----	---	---	Noisy
			OIV]/SiIV λ1400	3866	9010	---	---	
			CIV λ1549	4276	3970	108	---	
1405-287	0.574	5	MgII λ2798	4406	3540	56	100	
			[OII] λ3727	5868	660	6	7	
			[NeIII] λ3869	6090	940	8	8	
			HI λ4102	6449	1860	13	11	
1406-076	1.494	4	CIII] λ1909	4756	5800	40	110	
			CII] λ2326	5807	2220	9	21	
			MgII λ2798	6982	3650	64	100	
1424-11	0.806	4	MgII λ2798	5048	5250	56	100	
			[NeV] λ3426	6192	2210	3	4	
1425-274	1.082		MgII λ2798	5826	3090	28	---	1 line
1427+109*	1.71		CIV λ1549	4190	----	---	---	
			CIII] λ1909	5125	----	---	---	
1430-178*	2.326	5	OVI λ1034	3433	4080	33	87	
			HI λ1216 / HI λ1240	4049	4900	242	430	
			CIV λ1549	5163	1980	56	100	
			HeII λ1640	5445	2090	14	22	
1434-076*	0.697		MgII λ2798	4748	4810	85	---	1 line

Table 1 – *continued*

Object	Redshift	Ref.	Line	Peak Wavelength Å	FWHM kms-1	W Å$^{\lambda}$	Relative Flux	Notes
1448-232	2.215	16	HI λ1216	3917	4175	120	330	SB, BW
			NV λ1240	3995	4500	48	130	
			SiII λ1264	----	----	7	20	
			OI λ1304	4200	2330	11	27	
			OIV]/SiIV λ1400	4513	6430	18	39	
			CIV λ1549	4978	4400	45	100	
			CIII] λ1909	6122	4400	35	70	
1452-217	0.780	16	MgII λ2798	4974	2710	26	---	
			[NeV] λ3426	6095	----	---	---	
			[OII] λ3727	6640	----	---	---	
1502+106*	0.563	5	MgII λ2798	4383	3880	57	100	
			HeII λ3220	5020	1370	7	9	
			[NeV] λ3426	5355	2330	31	38	
1508-055	1.185		CIV λ1549	3382	1680	35	100	
			CIII] λ1909	4172	2160	22	33	
			MgII λ2798	6122	2230	23	22	
1510-08	0.362		MgII λ2798	3802	2680	29	100	
			HI λ4340	5913	3380	38	40	
			HI λ4861	6603	2580	31	37	
			[OIII] λ4959	6768	----	---	---	
			[OIII] λ5007	6813	----	---	---	
1511-10	1.513		CIV λ1549	3901	4280	132	100	
			HeII λ1640	4122	3190	11	8	
			CIII] λ1909	4782	8570	40	26	
			MgII λ2798	7042	6440	83	48	
1532+01/2	0.310	15	HeII λ3220	4199	2951	13	110	
			[NeIII] λ3869	5059	770	8	48	
			[NeIII] λ3968	5231	1040	4	20	
			HI λ4102	5679	3560	24	110	
			HI λ4861					
			[OIII] λ4959	6366	3370	75	320	
			[OIII] λ5007	6550	780	28	100	
1542+042*	2.184	5	HI λ1216	3872	3570	248	680	NV Weak
			OI λ1304	4195	2750	39	73	
			OIV]/SiIV λ1400	4468	2290	12	22	
			CIV λ1549	4929	2190	42	100	
1556-245	2.813	5	HI λ1216	4637	----	---	---	
			CIV λ1549	5905	----	---	---	
1614+051*	3.210		CIII λ 977	4114	2730	9	4	
			OVI λ1034	4349	5020	59	22	
			HI λ1216	5123	3310	325	100	NV Weak
1618+177* (3CR334)	0.554		MgII λ2798	4346	7350	93	---	
1655+077*	0.621		CII] λ2326	3758	5090	70	150	At end of scan
			MgII λ2798	4552	2080	45	100	
1656+053	0.887	4	CII] λ2326	4389	4610	4	15	
			MgII λ2798	5277	3580	29	100	
1705+018	2.569	4	HI λ1216	4344	3800	350	760	SB, BW
			NV λ1240	4423	4010	63	130	
			SiII λ1264	----	----	31	---	
			OI λ1304	4664	2770	19	35	
			OIV]/SiIV λ1400	4997	4230	20	32	
			CIV λ1549	5522	3010	82	100	
			CIII] λ1909	6802	3210	27	18	

Table 1 – *continued*

Object	Redshift	Ref.	Line	Peak Wavelength Å	FWHM kms-1	W Å$^{\lambda}$	Relative Flux	Notes
1725+044	0.296	4	HI λ4102	5308	3670	10	15	
			HI λ4340	5627	5280	24	37	
			HI λ4861	6303	3070	61	100	
			[OIII] λ4959	6430	1540	10	16	
			[OIII] λ5007	6488	1480	33	50	
1743+173*	1.702		CIV λ1549	4179	2800	146	100	
			CIII] λ1909	5166	3200	51	30	
1756+237	1.719		CIV λ1549	4203	3810	33	100	
			CIII] λ1909	5208	7310	4	40	
1912-549	0.402	3	MgII λ2798	3916	4890	15	100	
			[NeIII] λ3869	5419	1990	5	17	
			[NeIII] λ3968	5550	----	---	---	
			HI λ4102	5793	----	---	---	
			HI λ4340	6105	1580	8	25	
			HI λ4861	6799	5570	64	180	
			[OIII] λ4959	6943	1550	21	56	
			[OIII] λ5007	7010	1110	25	66	
1929-457	0.653	3	MgII λ2798	4624	5420	66	---	
			[OII] λ3727	6145	----	---	---	
			[NeIII] λ3968	6580	----	---	---	
1942-571*	0.529	14	MgII λ2798	4273	3930	41	100	
			HI λ4340	6642	7980	---	---	
			HI λ4861	7435	3730	72	76	
1954-388	0.626	14	MgII λ2798	4550	3230	33	---	1 line
2002-185	0.859		CIII] λ1909	3545	6470	---	---	
			MgII λ2798	5204	6430	94	---	
2008-159	1.178	4	CIII] λ1909	4149	8620	45	120	
			MgII λ2798	6105	4140	47	100	
2020-370	1.047	1	CIII] λ1909	3904	6600	36	150	
			MgII λ2798	5735	3120	39	100	At end of scan
2024-217	0.463	1	MgII λ2798	4090	4470	125	100	
			[NeV] λ3426	5013	2330	20	15	
			[OII] λ3727	5453	1100	19	11	
2037-253	1.574		OIV]/SiIV λ1400	3615	2160	29	24	
			CIV λ1549	3985	3010	138	100	
			CIII] λ1909	4900	5160	43	23	
2044-168*	1.937	1,9,14	HI λ1216	3576	3000	180	210	SB, BW
			NV λ1240	3644	4300	70	82	
			SiII λ1264	----	----	18	21	
			OIV]/SiIV λ1400	4116	4820	5	7	
			CIV λ1549	4553	2900	122	100	
			CIII] λ1909	5598	4950	30	29	
2053-045	1.177		CIII] λ1909	4150	4370	37	160	
			MgII λ2798	6099	1720	42	100	
2058-425	0.220	3	[NeIII] λ3869	4701	1500	7	50	
			[NeIII] λ3968	4850	1600	3	20	
			HI λ4102	5013	1400	6	40	
			HI λ4861					
			[OIII] λ4959	5941	4000	34	190	
			[OIII] λ5007	6115	1300	17	100	

Table 1 – *continued*

Object	Redshift	Ref.	Line	Peak Wavelength Å	FWHM kms-1	W Å$^{\lambda}$	Relative Flux	Notes
2112-407*	2.546		OVI λ1034	3677	2050	22	25	OS
			HI λ1216	4310	4550	334	330	SB
			NV λ1240	----	----	40	40	
			SiII λ1264	----	----	20	21	
			OIV]/SiIV λ1400	4966	5110	23	17	
			CIV λ1549	5493	4990	123	100	
			HeII λ1640	5797	1340	12	9	
2126-158*	3.264	3,8	OVI λ1034	4360	2490	10	19	
			HI λ1216	5198	4320	125	270	SB
			NV λ1240	5289	2940	50	110	Uncertain
			SiII λ1264	----	----	20	44	
			OI λ1304	5590	2320	---	---	
			OIV]/SiIV λ1400	5981	6530	12	24	
			CIV λ1549	6587	5850	60	100	
2135-248	0.821	4	MgII λ2798	5096	13000	64	---	1 line
2142-75	1.138	3	CIII] λ1909	4073	4920	24	150	
			MgII λ2798	5992	2760	21	100	
2143-156/R	0.701	1,15	MgII λ2798	4759	2810	34	---	1 line
2143-156/2	2.054	1,15	HI λ1216 / NV λ1240	3718	----	298	350	
			OI λ1304	4003				
			OIV]/SiIV λ1400	4296	3120	20	19	
			CIV λ1549	4727	3740	105	100	
2144-362	2.084	3	CIV λ1549	4775	4460	84	---	
			CIII] λ1909	5895	----	---	---	
2149-306*	2.345		HI λ1216	4073	2860	69	220	SB
			NV λ1240	4131	2940	35	110	Uncertain
			SiII λ1264	----	----	12	38	
			OIV]/SiIV λ1400	4694	4330	8	25	
			CIV λ1549	5162	6400	30	100	
			CIII] λ1909	6380	2750	---	---	
2153-209*	1.843	11	CIV λ1549	4396	6250	59	100	OS
			CIII] λ1909	5437	6520	40	50	Very noisy
2154-325*	1.819		CIV λ1549	4355	3030	66	100	
			CIII] λ1909	5394	7770	46	45	Very noisy
2158-214*	2.078	11	HI λ1216	3737	5650	90	320	OS, SB
			NV λ1240	3831	3650	45	130	
			SiII λ1264	----	----	---	---	
			OI λ1304	4030	3210	14	40	
			CIV λ1549	4762	7550	50	100	
			CIII] λ1909	5888	7050	40	59	
2159-194	1.172	11	CIII] λ1909	4133	7380	28	160	OS
			MgII λ2798	6080	4290	41	100	
2200-238	2.120	3, 10	HI λ1216	3794	3680	163	270	SB
			NI λ1240	----	----	41	68	
			SiII λ1264	3950	1290	7	11	
			OI λ1304	4065	1180	3	5	
			CII λ1335	4189	----	--	---	
			CIV λ1549	4832	2420	97	100	
			HeII λ1640	5130	1380	4	5	
			CIII] λ1909	5950	4180	35	30	
2202-185	1.809	11	CIV λ1549	4351	8100	166	100	OS
			CIII] λ1909	5361	4560	42	15	
2203-188	0.619		MgII λ2798	4539	4440	62	100	
			HeII λ3220	5207	860	3	6	
			[NeV] λ3426	5542	1730	5	8	

Table 1 – *continued*

Object	Redshift	Ref.	Line	Peak Wavelength Å	FWHM kms-1	W Å$^{\lambda}$	Relative Flux	Notes
2204-54	1.206	14	CIII] λ1909	4196	7120	32	180	
			MgII λ2798	6192	3360	51	100	
2204-191	1.068	11	MgII λ2798	5782	2880	28	---	1 line, OS
2205-196	1.283	11	CIII] λ1909	4350	7610	41	190	OS
			CII] λ2326	5314	2340	7	19	
			MgII λ2798	6396	4100	34	100	
2206-199	2.544	11	HI λ1216 / NV λ1240	4346	----	311	500	OS
			OIV]/SiIV λ1400	4939	8010	34	50	
			CIV λ1549	5498	10270	82	100	1 line redshift
2206-180	1.068	11	CIII] λ1909	3942	----	---	---	OS
			MgII λ2798	5793	5210	44	---	
2206-187	2.161	11	OI λ1304	4114	2870	21	61	OS
			OIV]/SiIV λ1400	4430	5020	17	33	
			CIV λ1549	4893	3490	69	100	
			CIII] λ1909	6034	4200	45	48	
2207-201	2.058	11	CIV λ1549	4737	9440	97	---	OS
2208-137	0.393	1, 10	MgII λ2798	3898	4580	31	---	1 line
2209-187	2.094	11	HI λ1216	3760	2870	119	360	OS, SB, BW
			NV λ1240	3841	3950	36	110	
			SiII λ1264	----	----	18	54	
			CIV λ1549	4793	3910	86	100	
			CIII] λ1909	5909	3860	56	54	
2210-25	1.833	10	HI λ1216	3443	2530	120	160	BW, RC
			NV λ1240	3508	4270	35	50	
			SiII λ1264	3590	1420	11	14	
			CIV λ1549	4386	3080	83	100	
2211-192*	1.953	11	CIII] λ1909	5636	6040	28	---	OS
2212-199	2.019	11	OIV]/SiIV λ1400	4226	5360	45	74	OS
			CIV λ1549	4673	7060	73	100	
			CIII] λ1909	5770	6900	33	37	
2212-299*	2.704	3,9,10	OVI λ1034	3810	3950	44	110	
			HI λ1216	4501	2730	181	390	SB, BW
			NV λ1240	4582	3590	45	100	
			SiII λ1264	----	----	14	32	
			OI λ1304	4836	2110	6	12	
			CII λ1335	4953	----	---	---	
			OIV]/SiIV λ1400	5180	3990	9	14	
			CIV λ1549	5734	2980	76	100	
			CIII] λ1909	7079	4730	49	47	
2213-202	1.046	11	CIII] λ1909	3906	1920	7	63	OS
			MgII λ2798	5726	6290	32	100	
2214-208	1.678	11	CIV λ1549	4146	5570	36	100	OS
			CIII] λ1909	5097	4340	26	40	
2227-08	1.561	10	CIV λ1549	3966	3330	92	100	
			HeII λ1640	4204	2110	7	7	
			CIII] λ1909	4888	2980	23	23	
2232-211/R	1.443		OIV]/SiIV λ1400	3398	2280	10	54	
			CIV λ1549	3786	4240	22	100	
			CIII] λ1909	4663	6820	26	82	

Table 1 – *continued*

Object	Redshift	Ref.	Line	Peak Wavelength Å	FWHM kms-1	W Å$^{\lambda}$	Relative Flux	Notes
2244-372	2.252		HI λ1216 } NV λ1240 }	3957	----	---	---	
			CIV λ1549	5031	----	---	---	
2245-128	1.892		HI λ1216 } NV λ1240 }	3520	----	---	---	
			OIV]/SiIV λ1400	4046	5240	26	63	
			CIV λ1549	4481	5590	44	100	
			CIII] λ1909	5514	4050	25	55	
2245-328/R*	2.27	4	HI λ1216	3984	6290	75	160	SB, BW
			NV λ1240	4052	7890	30	66	
			OIV]/SiIV λ1400	4555	5700	22	39	
			CIV λ1549	5030	9000	68	100	
			CIII] λ1909	6242	7060	36	38	
2246-309	1.302	1	CIV λ1549	3559	6420	152	100	
			CIII] λ1909	4400	6660	62	18	
2255-282	0.925	1,14	CIII] λ1909	3671	4330	29	160	
			MgII λ2798	5389	3450	38	100	
2257-270	1.481		CIV λ1549	3840	3510	230	100	
			CIII] λ1909	4740	2410	97	32	
2300-18	0.128	3,10	[OII] λ3727	4205	----	---	---	N galy.?
			[NeIII] λ3869	4365	----	---	---	
			HI λ4340	4904	2850	18	40	
			HI λ4861	5480	3720	47	100	
			[OIII] λ4959	5593	860	38	80	
			[OIII] λ5007	5646	740	94	190	
2300-683	0.515	3	MgII λ2798	4233	2970	38	100	
			HI λ4340	6587	6110	19	17	
			HI λ4861	7362	3010	---	---	At end of scan
2302-279	1.434	4	CIV λ1549	3749	7480	74	100	
			CIII] λ1909	4648	9490	40	31	
			MgII λ2798	6805	4100	17	10	
2303-052	1.136	4,10	MgII λ2798	5969	3460	59	---	1 line
2310-322	0.337	14	MgII λ2798	3760	6540	31	100	
			[OII] λ3727	4980	1660	3	5	
			HI λ4861	6500	7150	95	105	
			[OIII] λ4959	6612	1860	9	13	
			[OIII] λ5007	6673	1340	48	53	
2314-116	0.550	3	MgII λ2798	4331	6161	34	---	
			[NeV] λ3426	5325	----	---	---	
			[NeIII] λ3869	6010	----	---	---	
			[NeIII] λ3968	6130	----	---	---	
2325-150	2.465	10	OVI λ1034	3579	6410	138	35	
			HI λ1216	4214	3560	643	160	SB
			NV λ1240	4314	6630	77	19	
			SiII λ1264	----	----	71	18	
			OI λ1304	4543	1460	17	5	
			OIV]/SiIV λ1400	4854	4270	27	7	
			CIV λ1549	5372	4190	308	100	
2326-477	1.300	2	CIII] λ1909	4386	8540	28	130	
			MgII λ2798	6444	2940	31	100	

Table 1 – *continued*

Object	Redshift	Ref.	Line	Peak Wavelength Å	FWHM kms-1	W Å$^{\lambda}$	Relative Flux	Notes
2329-16	1.155	10	CIV λ1549	3337	2880	103	100	
			CIII] λ1909	4114	2480	127	74	
			MgII λ2798	6029	3330	84	79	
2329-384*	1.20		CIV λ1549	3459	9160	95	100	
			CIII] λ1909	4170	7140	50	33	
			MgII λ2798	6145	7070	34	15	
2335-18	1.439	1,10	CIV λ1549	3766	6870	29	100	
			CIII] λ1909	4672	6960	29	58	
2351-154	2.67	4,10	HI λ1216	4471	4440	150	540	BW
			NV λ1240	4557	4800	40	180	Uncertain
			CIV λ1549	5666	2530	50	100	
			HeII λ1640	6058	1300	10	22	
			CIII] λ1909	7059	3000	20	36	
2352-342	0.706	3	MgII λ2798	4765	4620	66	100	At end of scan
			[NeIII] λ3869	6594	1500	10	7	
2355-106	1.626		OI λ1304	3440	2100	6	7	
			CII λ1335	3546	1710	4	4	
			OIV]/SiIV λ1400	3682	2120	9	9	
			CIV λ1549	4070	4540	102	100	
			CIII] λ1909	5004	5720	19	14	
2358-161	2.033	10	HI λ1216	3688	6950	188	300	SB
			NV λ1240	3744	7490	100	160	
			SiII λ1264	----	----	19	30	
			OIV]/SiIV λ1400	4263	6360	17	22	
			CIV λ1549	4702	7090	84	100	
			HeII λ1640	5020	3380	---	---	
			CIII] λ1909	5759	12330	38	36	

References:
1. Peterson *et al.* (1976).
2. Wright *et al.* (1977).
3. Jauncey *et al.* (1978a).
4. Peterson *et al.* (1979).
5. Wright *et al.* (1979c).
6. Wright *et al.* (1978).
7. Peterson *et al.* (1978).
8. Jauncey *et al.* (1978b).
9. Wilkes (1984).
10. Wright, Ables & Allen (1983).
11. Savage *et al.* (1978).
12. Wright *et al.* (1979a).
13. Wright, Peterson & Jauncey (1979b).
14. Browne, Savage & Bolton (1975).
15. Bolton *et al.* (1976).
16. Browne & Savage (1977).

The redshift was estimated from the peak wavelengths of those lines which were positively identified; the low-ionization lines O Iλ1304 and C IIλ1335 were excluded from this determination since they are believed to be redshifted relative to the high-ionization lines (Gaskell 1982, Paper I). The O IV]/Si IVλ1400 feature was also excluded since the two emission lines are heavily blended, so that their relative strengths and hence their expected rest frame wavelength are undetermined.

The FWHM is commonly used as an indicator of the velocity dispersion of an emission line. Many factors affect the accurate measurement of this parameter, in particular the amount of depression of the peak height due to the combined effects of low-resolution, poor S/N and uncertainty in the adopted continuum level. The likely measurement error, estimated by measuring the FWHM for the highest and lowest plausible continuum levels, was generally 5–30 per cent for strong lines. The error can be much greater than this for weak, noisy and/or absorption-contaminated lines. The reliability of each measurement can best be judged by inspecting the observed line profile in WWJP.

In order to obtain parameters for Lyα and the doublet N Vλ1240 blended into its red wing, it was necessary to deblend the lines in some way. The degree of blending of the two features varies according to their relative strengths and FWHM. One or more of the following procedures was used for deblending, depending upon the nature of the data. The method used is indicated in Table 1.

(i) When the peaks were well resolved and it was possible to trace the shape of the red wing of Lyα, a continuum was fitted through this wing. The N V and, if present, Si IIλ1264 features were then isolated and measured following the regular procedure. This method was used only when the lines were relatively narrow (FWHM $\lesssim$4000 km s^{-1}) and N V strong [I(N V) $\gtrsim$30 per cent I(Lyα)] and thus is not expected to lead to any measurement errors additional to those for unblended lines.

(ii) When the degree of blending was too great for (i), two alternative methods were used, in conjunction where possible, their relative success being dependent upon the quality and nature of the data. In a number of objects no deblending was possible due to poor data or unusual line profiles in which case measurements for the combined profile are given in Table 1.

(a) A synthetic blend was generated using an unblended line profile from the same spectrum (usually C IVλ1549) as a prototype (see Paper I, Wilkes & Carswell 1982). The presence of absorption in the blue wing of Lyα was allowed for as far as possible. An individual component could then be isolated by subtracting the synthesis of the other components from the observed feature. When there was a velocity difference between the peak positions of Lyα and the prototype, a compensating shift was applied when generating the synthesis; it is the shape of the profile not its absolute position which is important for this procedure. This method relies upon the profiles of all the composite lines being similar to that of the prototype. This is generally true to within ~10 per cent in high-resolution data, i.e. frequently not detectable in low-resolution data. For a few unusual objects where the profiles were clearly different the method was not used. Thus errors at <10 per cent level are expected in combination with those due to continuum uncertainty and the possible presence of weak emission and absorption features that plague all profile measurements (see discussion in Wilkes & Carswell 1982).

(b) The blue wing of Lyα, with any obvious narrow absorption lines removed, was reflected about the peak forming a symmetric profile which was then subtracted to isolate N V and Si II. Additional sources of error for this method are the depression of the Lyα blue wing by blended narrow absorption lines which can amount to ~10 per cent of the total line flux in low-resolution data, the uncertainty in the peak position of Lyα, particularly when the N V flux

is relatively high, and the use of a symmetric Lyα profile (generally true to within the margin of errors, Wilkes & Carswell 1982). The position about which the Lyα profile was reflected was adjusted to fit the core and extreme wings of the profile where N v contributes less flux. The method was not employed where the line profiles were clearly asymmetric or the N v flux too strong to allow a reasonable fit.

The results are displayed in Table 1 as follows: Column 1: coordinate designation of QSO (/2 indicates a radio-quiet object near the radio source found during the search for the optical identification of that source); column 2: mean redshift as determined from the peak positions of the unblended emission lines; column 3: references to the original papers reporting these data (additional references are given by WWJP and will not be repeated here); column 4: name and rest wavelength (Å) of emission line; column 5: observed peak wavelength (Å); column 6: Rest-frame FWHM in km s^{-1}; column 7: observed equivalent width (Å); column 8: relative flux; column 9: notes. The following coding has been utilized in the notes: OS = optically selected; SB = use of a synthetic blend to deblend Lyα, N v (see above); BW = reflection of blue wing of Lyα; RC = fitting of continuum through the red wing. The flux (column 8) was measured relative to a reference line fixed arbitrarily at a flux of 100; C IVλ1549, Mg IIλ2798 or H$\beta\lambda$4861 were used where possible. Any notable peculiarities or measurement problems are given below for objects indicated by '*' in Table 1. It should be noted that, since the spectral resolution is generally 300–900 km s^{-1} (see WWJP), any features having FWHM $\lesssim$1200 km s^{-1} are at best marginally resolved.

4 Notes on individual objects

0002−422. N v peak appears redshifted due to absorption on the shortward side.

0008−264. The C III] equivalent width is unusually high. An alternative redshift is 1.572 with C IV at 3984 Å.

0029−414. Mg II is redshifted ~1800 km s^{-1} relative to C III].

0036−392. Hump at blue end is due to poor flux calibration.

0046−315. N v flux uncertain due to absorption.

0048−071. Lyα, N v, Si II fluxes are inaccurate due to uncertain continuum shortward of this feature.

0049−393. This QSO is unusual in several respects. First, there is a strong broad absorption line shortward of C IV by ~300 Å and no corresponding absorption for the other emission lines. Secondly, He II appears very strong and broad, probably due to blending with Fe II emission (Gaskell 1981). Thirdly, the emission line peaks do not line up, the simplest interpretation being that strong N v [0.5*I(Lyα)] has shifted the apparent peak of Lyα and that the O VI line is predominantly Lyβ. The spectrum also shows an absorption system at z = 2.792 containing N v, Si II, C IV but no apparent Lyα lines. A spectrum was also presented by Whelan, Smith & Carswell (1979) who determine a redshift of 2.85 from Lyα, C IV.

0054−006. N v, Si II fluxes uncertain due to absorption.

0150−334. This object has two possible redshifts: 0.610, in which case [Ne v] and [O II] appear broader than normal; or 1.907, the features being C IV, C III] and a third which is unidentified at 2060 Å rest wavelength.

0234−301. C IV is significantly blueshifted with respect to Lyα and is broader, suggesting that Lyα is more severely affected by absorption than it appears at this low resolution.

0254−334/R. C IV appears broader than Lyα and has a red asymmetry (unusual, see Young, Sargent & Boksenberg 1982, and Paper I), it may be due to Fe II emission. N v is weak, <10 per cent Lyα flux.

0254−334/2. This QSO, ~1.2 arcmin from the radio source, has been classified as a broad absorption line object. The emission lines are difficult to measure at low resolution, values here are quoted for the emission longward of the absorption trough.

0329−255. N v is unusually strong, the peak position of Lyα was estimated by deblending the feature.

0414−189. Redshift revised since earlier reference, see WWJP.

0448−187. Only one clear line, identified as C IV because of suggestion of Lyα emission ~3710 Å.

0537−441. BL Lac? See reference.

0537−286. A strong Lyman limit jump is present at a redshift of 2.984.

0723−008. The H$\beta\lambda$4861 profile is broad and severely blended with [O III]λ4959; no measurement was possible. There is also a strong, unidentified narrow peak ~5000 km s^{-1} shortward of Hβ; this may be a displaced narrow component as observed, e.g. in 3C 227 (Osterbrock, Koski & Phillips 1976).

0748+126. Four lines are reported by Wills & Wills (1976) confirming this redshift.

0858−77. Lines are weak and hard to measure. [O III] doublet is blended together and at end of scan.

1111+149. Wills & Wills (1976) report the same redshift based upon two lines.

1117−248. Mg II, Hβ features possess a narrow component which is included in the profile measurements.

1146−037. Hβ is broad and blended with the [O III] doublet, making profile measurements very uncertain.

1148−171: 1216 blend is on the end of the scan making measurements inaccurate.

1151−34. Hβ is too broad to measure.

1157+014. C IV is contaminated by two strong absorption features, flux and equivalent width estimates were not possible.

1158+007. Mg II is redshifted ~3000 km s^{-1} relative to C III], an unusually large shift.

1200−051. No [O III]λ4959 is apparent.

1215+013. Lines very weak, may be galaxy.

1311−270. C IV line peak is blueshifted ~800 km s^{-1} relative to that of Lyα, this may be due to absorption in the red wing of C IV.

1327−214. With the exception of Mg II, the lines are weak and noisy.

1336−000. Wills & Lynds (1978) report $z=0.558$ based upon one line only.

1355−41. Hβ and [O III]$\lambda\lambda$4959, 5007 are severely blended.

1427+109. Alternatively lines may be identified as Mg II and [Ne v]λ3426, yielding a redshift of 0.495.

1430−178. The continuum shortward of Lyα is highly uncertain. N v is weak or negligible. Night sky emission is present at 5577 Å.

1434−076. [Ne v]λ3426 may be present at 5800 Å.

1502+106. This QSO has two possible redshifts, the second being 1.833 with the 4383 Å line identified as C IV (Smith *et al.* 1977). The Mg II and Ne v identifications fit the measured wavelengths in this spectrum better than C IV and C III]. However the higher redshift would identify the feature ~3450 Å as Lyα rather than poor continuum calibration. (See also discussion by Wright *et al.* 1979c).

1542−042. N v is weak or negligible.

1614+051. N v is too weak to measure.

1618+177. Although only one line is reported here, this object has been heavily studied and the redshift is well known (e.g. Lynds, Stockton & Livingstone 1965).

1655+077. Also observed by Kuhr, Liebert & Strittmatter (1985, in preparation), who found no C II] line.

1743+173. Night sky emission is present at 5577 Å.

1942−571. Hβ emission is at the end of the scan, measurements are uncertain.

2044−168. The C IV profile is narrow and red asymmetric suggesting absorption in its blue wing. This is confirmed in high-resolution data (Paper I).

2112−407. Both C IV and Lyα have strong, possibly broad absorption in their blue wings. N V, Si II fluxes are inaccurate.

2126−158. The peculiar shape of C IV, used as the prototype profile, and absorption in the blue wing of Lyα render measurements of N V, Si II inaccurate. O VI is substantially blueshifted, suggesting a strong Lyβ component, although the presence of absorption in the red wing may contribute to the shift. O Iλ1304 flux was not measured due to strong absorption.

2149−306. The irregular profile of C IV and absorption in the blue wing of Lyα cause uncertainty in N V, Si II measurements. C IV appears to be blueshifted $\sim$1400 km s^{-1} with respect to Lyα.

2153−209. Alternatively, the line at 4400 may be Mg II, giving a redshift of 0.571.

2154−325. Alternatively, the line at 4355 may be Mg II, giving a redshift of 0.556.

2158−214. The proximity of the 1216 blend to the short-wavelength end of the scan renders measurements of its components inaccurate.

2211−192. This redshift is highly uncertain due to weak, noisy lines.

2212−299. The sharp blue wing of Lyα suggests absorption, this is confirmed in high-resolution data (Paper I).

2245−328/R. C IV and 1400 Å are unusually strong and blueshifted with respect to the 1216 blend. Deblending was performed by assuming the peak was due to Lyα. However, an alternative interpretation is that the blend is predominantly N V emission.

2329−384. C IV is apparently redshifted. Since it was observed at a different date from the remainder of the spectrum, it is possible that the wavelength scales are not relatively correct.

5 Results

The full sample of 295 QSO candidates, presented in WWJP, includes 81 objects with no measurable emission lines. The majority of these have low-quality spectra, only 22 being strong BL Lac candidates. Active galaxies with weak or no emission lines may represent a large fraction of the class, but no quantitative statement concerning the fraction of BL Lac objects in an unbiased sample can be made until the objects in question are positively identified. It should be noted that, due to the non-uniformity of the spectral data across the sample, it is not complete down to any specific equivalent width or line flux limit.

Emission line strengths are of great importance both in comparing different samples of QSOs and in modelling the physical conditions of the emitting gas. In Table 2 the distribution of equivalent widths for the broad and narrow lines is detailed as follows: Column 1: name and rest wavelength (Å) of emission line; columns 2, 3, 4: mean equivalent width, standard deviation (Å) and the total number of objects used in the distribution; column 5: number of objects in which the line fell in the observed wavelength range but was undetected. This last number gives an indication of the effect on the distribution due to the ill-defined lower limit on detectable equivalent width of an emission line. In Table 3 the distributions of various line intensity ratios are listed: Column 1: line ratio; columns 2, 3, 4: total number of objects, mean and standard deviation for each intensity ratio; column 5: notes. The mean ratios are in general agreement with those of Baldwin (1975, 1979). No significant difference was found between the distributions of

Table 2. Distribution of rest-frame equivalent widths for prominent broad and narrow lines.

Line	Parameters of Distribution			N
	W_λ/Å	σ/Å	n	
OVI λ1034	15	13	12	0
Lyα 1216	65	34	38	0
NV λ1240	19	9	34	2
SiII λ1264	7	5	21	13
OI λ1304	4	3	14	40
OIV]/SiIV λ1400	6	3	41	17
CIV λ1549	32	20	94	4
HeII λ1640	4	3	12	5
CIII] λ1909	17	12	96	8
CII] λ2326	4	3	7	41
MgII λ2798	27	15	113	2
[NeV] λ3426	6	6	18	53
[OII] λ3727	8	6	23	25
[NeIII] λ3869	5	2	21	21
Hβ λ4861	47	25	26	8
[OIII] λ5007	32	28	30	2

Table 3. Parameters for intensity ratio distributions of the prominent broad lines.

Ratio	n	$\bar{x}$	σ	Notes
I(OVI)/I(Lyα)	11	0.18	0.11	Contaminated by absorption
I(NV)/I(Lyα)	33	0.32	0.13	
I(SiII)/I(Lyα)	20	0.10	0.05	
I(OI)/(CIV)	15	0.23	0.21	
I(CII)/I(CIV)	5	0.07	0.03	
I(1400)/I(CIV)	41	0.25	0.16	
I(CIV)/I(Lyα)	39	0.36	0.16	
I(CIII])/I(CIV)	62	0.40	0.19	
I(MgII)/I(CIII])	42	0.89	0.46	
I(Hβ)/I(MgII)	14	0.87	0.50	Problems due to blended [OIII] Lines

equivalent width or line intensity ratios of optically and radio-selected objects in this sample. The numbers quoted refer to all the available objects.

The number versus redshift distribution for the sample is displayed in Fig. 1. The strong peak at $z\sim2$ found in objective prism surveys (Osmer & Smith 1980) is notably absent. There is a bias towards low-redshift, only three objects having $z>3$, which is typical of radio-selected samples

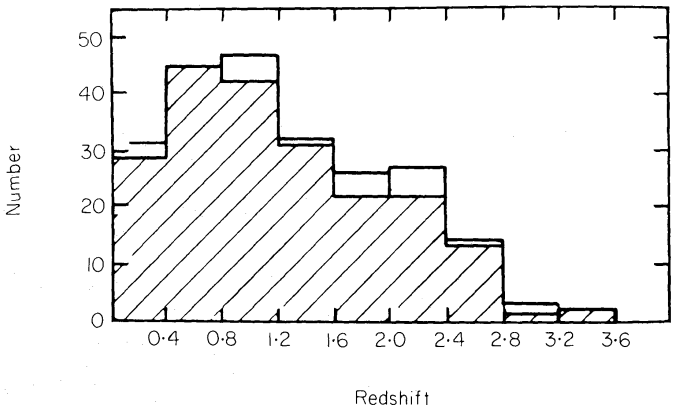

Figure 1. Number–redshift distribution of the sample [optically selected (OS) objects are unshaded].

(Smith 1982). The lack of high-redshift objects in radio-selected samples of QSOs was originally thought to be due to the additional UVX criterion often used to distinguish between multiple candidates for optical identification (e.g. Baldwin *et al.* 1973). However, subsequent analysis with this bias removed failed to increase the number of radio-selected high-redshift QSOs substantially (Smith *et al.* 1977; Baldwin, Wampler & Burbidge 1976). Studies of extragalactic radio sources based upon very accurate positions also show a lack of high-redshift objects implying a real turn-over in the comoving space density of radio-loud QSOs (Peacock & Wall 1981). There is not expected to be a significant bias due to UVX selection in the present sample. Colour was used initially to supplement the 10 arcsec accuracy of the Parkes radio positions but follow up NRAO radio observations with 2-arcsec accuracy were also made (Peterson *et al.* 1976; Savage & Wright 1981).

An important property of any QSO sample in terms of modelling the BELR is the observed distribution of linewidths (Osterbrock 1977). Potentially, this could serve to distinguish between disc-like and spherical geometries for the emitting gas. The FWHM distribution of C IV, believed to be the only uncontaminated broad line in this sample, is shown in Fig. 2. Its nature appears similar to that presented by Baldwin (1979), the mean is 4500 km s^{-1} but a tail extends to large widths. It should be noted that the selection effect against finding weak, broad lines may affect this distribution, but not substantially, since C IV is a prominent emission line.

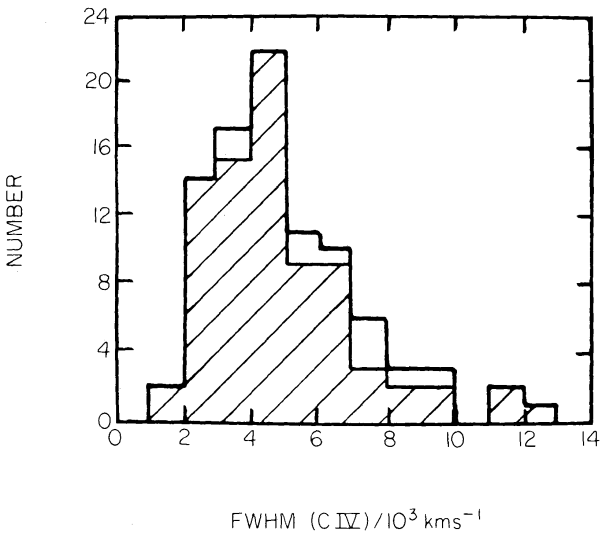

Figure 2. Distribution of full-width-at-half-maximum for the C IV emission line (OS unshaded).

6 Line positions

6.1 REDSHIFT OF LOW-IONIZATION LINES

Gaskell (1982) first noted a mean apparent redshift of the O Iλ1304 emission lines in high-redshift QSOs of $560\pm120\,\mathrm{km\,s^{-1}}$ with respect to C IV (the errors quoted here indicate the 1σ dispersion of the sample not the measurement error). This effect has been confirmed in high-resolution spectra of seven QSOs in Paper I, where a mean shift of $760\pm130\,\mathrm{km\,s^{-1}}$, with respect to the mean laboratory wavelength of O I, 1303.5 Å, was reported. If the same rest wavelength were used as in Gaskell's (1982) paper, i.e. 1304.36 Å, appropriate for optically thick gas, the shift reported in Paper I becomes $560\,\mathrm{km\,s^{-1}}$, in excellent agreement with Gaskell's result. In Table 4 the distribution of the mean shift in peak position of O Iλ1304 and C IIλ1335 with respect to that of C IV are tabulated for this sample. Column 2: reference line; columns 3, 4, 5: the mean shift standard deviation and number of objects for the distribution; column 6: significance of mean shift in terms of $\sigma/\sqrt{n}$. These measurements were again made relative to the mean laboratory wavelength of O I and so should be compared to the higher value quoted above. The mean shift for O I is $1290\pm180\,\mathrm{km\,s^{-1}}$, a factor of 1.7 higher than the earlier results. The two most discrepant O I profiles, those of 0819−032 and 1542+042, were omitted from this distribution to guard against misidentification. Their inclusion increases the mean shift to $1480\pm220\,\mathrm{km\,s^{-1}}$. Taking into account the widths of the two distributions, the more conservative estimate of $1290\pm180\,\mathrm{km\,s^{-1}}$ is 2.5σ higher than the earlier results. The small number of C II lines detected in this sample yield a shift in good agreement with that of O I, where highly discrepant line positions were again omitted from the distribution. Thus, the present data provide further confirmation that a shift of the low-ionization lines with respect to C IV is present and indicates that there is a large dispersion in the magnitude of this shift.

One possible interpetation for shifts of this nature is incorrect identification of the features, the measured mean line positions indicating intrinsic wavelengths of 1309.8 Å and 1343.2 Å respectively. As discussed by Gaskell (1982), the most likely contender for such a misidentification of the O I feature is a Si II doublet of mean wavelength 1307.66 Å. However, the weakness or absence of other associated Si II lines such as $\lambda\lambda$1196, 1264, 1531, 1817 Å argue against such an identification (Gaskell 1982; Dumont & Mathez 1981; Jordan 1969). The data presented here support this conclusion, in particular, the mean ratio of O Iλ1304 to that of Si IIλ1264 in the sample is 0.55 ± 0.41, a factor of 2 higher than predicted if the 1304 feature were due purely to Si II.

It has also been shown (Gaskell 1982) that Mg II is redshifted by $565\pm100\,\mathrm{km\,s^{-1}}$ relative to C IV. Its position relative to C III] in this sample indicates a similar shift ($600\pm90\,\mathrm{km\,s^{-1}}$, see Table

Table 4. Investigation of relative velocities of emission lines: parameters of distributions.

Line	Reference Line	Δv/kms^{-1}	σ/kms^{-1}	n	Signif.
OIλ1304	CIV	1290	800	19	7
CIIλ1335	CIV	1320	1046	7	3.3
CIVλ1549	CIII]λ1909	120	1200	65	0.5
MgIIλ2798	CIII]	600	600	44	6.7
MgIIλ2798	[OII]	-200	810	22	1
[OII]λ3727	[OIII]λ5007	100	310	6	1.3
HIλ4861	[OIII]λ5007	220	730	23	1.5

4). The C III] line was used as a reference line in this sample, since this increased the number of objects for which the position of Mg II could be compared with that of the higher ionization lines. The presence of a small but insignificant shift between the C IV and C III] lines suggests that the relative positions of C IV and Mg II in this sample are $\sim$100 km s^{-1} closer than Mg II and C III]. In either case the shifts are in excellent agreement with Gaskell's initial value. In the case of Mg II, the identity of the feature is not seriously in question, and the only alternative interpretation to a real velocity shift is that the apparent line peak is shifted due to blending with Fe II emission in the wings. Since Fe II emission is present in both wings and is substantially weaker than Mg II, this is unlikely (Gaskell 1982).

Assuming that the velocity shifts are real, we are immediately led to the question of which (if any) of the emission lines indicate the true redshift of the QSO (assuming the redshift is mainly cosmological). The relative positions, of Mg II, [O II]λ3727, [O III]λ5007 and Hβ were investigated for this sample. These results are also given in Table 4 and show that within the margin of errors, all these lines are at rest with respect to one another. In Seyferts and a few low-redshift QSOs it has occasionally been possible to measure the redshift of the underlying galaxy (Heckman *et al.* 1981); results so far indicate that the narrow lines are within $\sim$100 km s^{-1} of the system velocity although systematically blueshifted by a small amount. Assuming that low- and high-redshift QSOs behave alike in this respect, the lack of significant shifts between Mg II and the forbidden lines implies that Mg II also indicates the 'true' redshift of the system. This in turn leads to the conclusion that the high-ionization lines are blueshifted by $\sim$600 km s^{-1} with respect to the systemic velocity of the QSO (as discussed by Gaskell 1982). The larger velocity shift of O Iλ1304 and C IIλ1335 for the present sample implies that these lines may be redshifted with respect to the systemic velocity by a comparable amount.

The assumption that QSOs are alike at low and high redshift is drastic but necessary, particularly since there are no narrow lines in the visible region for high-redshift QSOs to use for confirmation of the relative line positions. To the best of my knowledge, there are no accurate measurements of the relative positions of O I, C IV, Mg II in the same QSO to confirm or negate the assumption. The large data bank of *IUE* observations is not useful in this case due to uncertainty in the zero-point of the wavelength scale which is generally 'overcome' by assuming the UV lines are at the *same* redshift as the optical.

Study of the relative profiles of emission lines from atoms in very different ionization states leads to information of the ionization equilibrium of the emitting gas as a function of velocity in the BELR. Subsequent modelling of gas velocity as a function of radius leads to spatial resolution which can be obtained in no other way. It is clear that shifts such as those reported above provide invaluable constraints on models. Possible interpretation in terms of radial motion and some form of obscuration has been discussed (Gaskell 1982; Wilkes & Carswell 1982, Paper I); extending these ideas to explain shifts in both directions, if the above results are confirmed, will complicate the situation considerably.

6.2 Lyα

Observers have often remarked on the slightly higher redshift of the Lyα over C IV emission lines. This effect has generally been attributed to a combination of blending with N V in the red wing and absorption in the blue wing. Gaskell (1982) investigated the shifts for a sample of published measurements and found a mean of 400$\pm$100 km s^{-1}. In the sample presented here a similar mean shift is present, 350$\pm$120 km s^{-1}, giving an effective rest wavelength for Lyα of 1217.1 Å, assuming C IV to be at 1549.1 Å.

The velocity separation of Lyα and N V is $\sim$6000 km s^{-1}, comparable with the velocity widths of the emission lines (mean $\sim$4500 km s^{-1}). One would expect that the apparent peak wavelengths

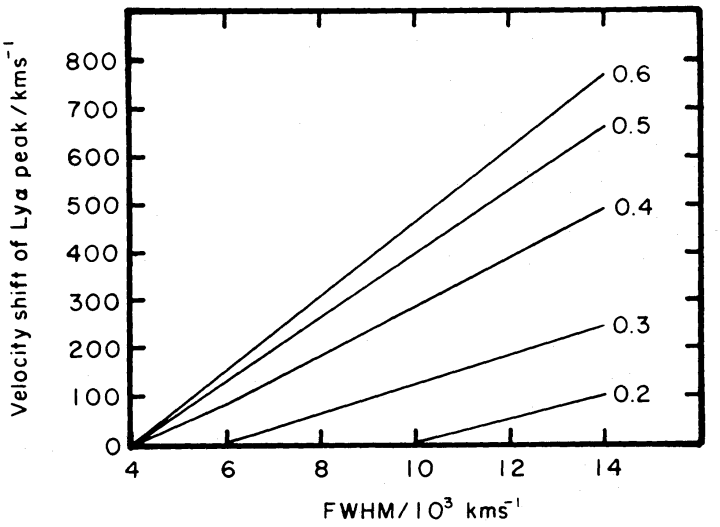

Figure 3. Predicted shift of the Lyα peak as a function of FWHM of the component lines for different strengths of N v relative to Lyα.

of the two lines would be shifted once the lines become severely blended, i.e. for broader lines and stronger N v flux. It is possible to make some prediction of the expected shift, as a function of N v strength and the FWHM of both lines, by synthesizing such a blend. In this procedure the Lyα and N v profiles were assumed to be identical and a 'typical', observed, high-resolution (1.5 Å) C IV profile was used as a prototype for both. A synthetic blend was generated by summing two prototype profiles with a specified FWHM and relative strength, positioned at the rest wavelengths of Lyα and N v respectively (see Wilkes & Carswell 1982). The position of the Lyα peak in the synthetic blend was then studied as a function of the FWHM and the relative strengths of the two lines. The results are displayed in Fig. 3 where the Lyα peak shift (in velocity units) is plotted as a function of FWHM for specified N v to Lyα flux ratio as labelled. Clearly, no shift is predicted for FWHM $<4000\,\mathrm{km\,s^{-1}}$ while for FWHM $>6000\,\mathrm{km\,s^{-1}}$ a shift is expected for any blend having an N v strength above the mean (30 per cent×Lyα, Table 3).

Table 5. Parameters describing the distribution of velocity shift of the Lyα emission line peak relative to C IV for FWHM$\gtrsim$5000 km s^{-1} and for I(N v)/I(Lyα)$\gtrsim$0.3.

Subset	z (Lyα) - z (CIV) /kms^{-1}	n	error ($\sigma/n^{\frac{1}{2}}$) /kms^{-1}
N	195	26	109
B	572	18	250
W	145	12	101
S	532	22	185
N+W	70	8	117
N+S/B+W	357	16	139
B+S	717	10	350

key: N = $\Delta v \leq 5000$ kms^{-1}

B = $\Delta v > 5000$ kms^{-1}

W = NV/Lyα < 0.3

S = NV/Ly$\alpha \geq 0.3$

To determine whether such an effect is occurring in the present dataset, the velocity of the Lyα profile with respect to that of C IV was studied as a function of FWHM and the relative strengths of N V and Lyα as follows: First, the sample was divided into two subsets according to FWHM (C IV)$\lessgtr$5000 km s^{-1}. Secondly, it was divided according to I(N V)/I(Lyα)$\gtrless$0.3. The parameters for the relative velocity distributions are given in Table 5 for all subsets. Clearly, a larger shift is observed, on average, for broader lines and strong N V, as expected from the above discussion. A highly significant difference is not expected: first, since the subsets describe two halves of a continuous distribution, and secondly, two effects are involved and they do not necessarily reinforce one another. The sample was divided further to distinguish those objects where both effects are reinforcing one another. The results are again shown in Table 5 and show the velocity shift increasing from 70 km s^{-1}, where the profiles are narrow and N V is weak, to 717 km s^{-1}, where they are broad and N V strong.

The large scatter inherent in the data precludes quantitative confirmation that N V blending is the dominant cause of the velocity shifts observed between the Lyα and C IV line peaks. However, the similarity between the predicted trends and those observed on the average in this dataset implies that the shifts can be explained in this way, i.e. there is no intrinsic difference in the velocities of the two lines.

6.3 C III]λ1909

This profile is believed to be blended in its blue wing with some combination of Si III]λ1892, Al IIIλ1858 and Fe IIλ1860 (Paper I, Gaskell, Shields & Wampler 1981; Wills, Netzer & Wills 1980). The S/N and resolution of the spectra in the sample are not high enough to detect this feature in individual cases (as in Paper I); however, cumulative evidence may be obtained from studying the distribution of FWHM and peak wavelength for the C III] profile. The FWHM distribution is shown in Fig. 4. It is broader than those of other unblended lines and has a mean of $\sim$5800 km s^{-1}, significantly larger than that of C IV (Fig. 2) at 99.4 per cent significance. Since both C IV and C III] emission originate in similar areas of the BELR (Kwan & Krolik 1981) it is unlikely that their velocity dispersion (and hence their line profiles) should be intrinsically so discrepant. This implies contamination of the C III] profile in one or both of its wings, confirming earlier results, but at a level insufficient to cause a shift in the peak wavelength, whose mean with respect to C IV in this sample is 1908.7 Å, in exact agreement with the laboratory wavelength.

The position of C III] has been reported to vary from object to object. Wills (1980) presented evidence from a large sample of 189 QSOs for a correlation betwen the peak wavelength of C III] measured with respect to C IV and the mean redshift of the QSO. In particular he found that

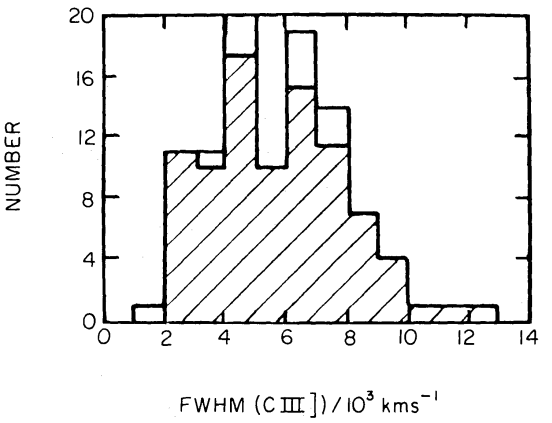

Figure 4. Distribution in FWHM of C III] across the sample (OS unshaded).

objects with $z>1.8$ have a higher effective wavelength than those with $z<1.8$ by 2.5 Å, a difference significant at the 4σ level. The mean effective wavelength for the objects in Wills' sample is 1908.25±0.28 Å, 2σ shortward of the laboratory mean. In contrast that of the present sample (60 objects) has a mean in exact agreement with the laboratory wavelength (see above).

To test for the Wills effect in this sample, the effective wavelength of C III] with respect to C IV is plotted as a function of mean redshift (Fig. 5). No correlation is apparent, the linear correlation coefficient for the data is 0.13 (30 per cent chance of random occurrence). Division of the sample into two subsets for $z \gtrless 1.8$, following Wills' method, yields no significant difference in their mean effective wavelength. This data sample does not display the same dependence between effective wavelength and redshift as that of Wills (1980). This is particularly surprising, since there is probably some overlap between the AAT data in Wills' sample, which gave a 2.4σ result, and those used here.

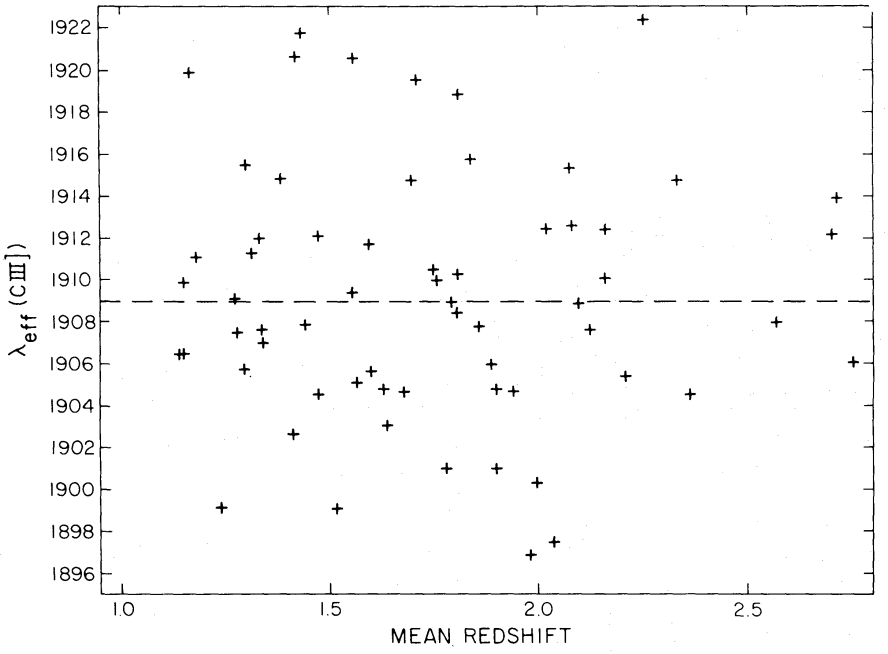

Figure 5. The effective wavelength of C III] (in Å) measured with respect to C IV as a function of mean redshift.

6.4 1400 Å BLEND

This feature was originally identified with the doublet Si IVλ1397. However, since the mean wavelength of the quintet O IV]λ1402 was revised from 1407 Å based on laboratory measurements by Bromander (1969), both features have been believed to contribute and their relative strengths have been the subject of some discussion. The distribution of published wavelengths was studied by Wills & Netzer (1979), who quote a mean wavelength of 1401.2±0.6 Å, implying that O IV] is the main contributor to the blend, while Young *et al.* (1982) find 1399.68±0.43 Å and Gaskell *et al.* (1981) 1399.8±0.5 Å, both implying roughly equal contributions from the two lines.

In this sample, the distribution of effective wavelength for the feature with respect to the mean redshift (computed without including the position of this blend) yields a mean wavelength of 1400.6±7 Å, in good agreement with the values mentioned above. This result indicates a mean intensity ratio of I(O IV]):I(Si IV)~2:1.

6.5 O VIλ1034/Ly$\beta\lambda$1025

This feature is buried in the Lyα forest of absorption lines and, even at high-resolution, the shape of the emission line is often unclear. its identity was originally believed to be O VI on theoretical grounds (Netzer 1976), although photoionization models had trouble reproducing its strength [$0.2\times I$(Lyα)]. However, more recent photoionization models predict the presence of Lyβ (Kwan & Krolik 1981) and, in addition, observational evidence for its presence in a number of spectra has been reported. The high-resolution studies in Paper I implied the presence of Lyβ in two of the three profiles studied. These results are based upon deblending the observed profile using that of C IV in the same object as a prototype. In addition, Green *et al.* (1980) make the same suggestion based upon the observed wavelength of the feature in five *IUE* spectra of low-redshift QSOs.

In this sample, the effective wavelength varies considerably from object to object (e.g. 1022.5 Å for 2126−158; 1035.3 Å for 0002−422). The mean for the 12 lines in the sample is 1031.5±1.2 Å, 3σ shortward of the laboratory mean wavelength of the doublet (1034.8 Å). If the highly discrepant position in 2126−158 is omitted, this mean increases to 1032.5±0.9 Å, still 2.6σ shortward. Although the result is not highly significant for this data set alone, it contributes to the mounting evidence that Lyβ contaminates the O VI emission line profile in a number of QSOs.

7 Conclusions

Emission line parameters for 214 radio-selected QSOs, covering a wide redshift range, have been presented. Preliminary studies of the sample, including FWHM and relative intensity distributions for the broad lines and equivalent width distributions for both broad and narrow lines, have been made.

The broad emission lines were studied in more detail and the following results obtained:

(i) Mg IIλ2798 is redshifted $\sim$600 km s^{-1} relative to the high-ionization lines in intermediate-redshift QSOs while it is at rest with respect to (wrt) the forbidden lines in low-redshift QSOs; this confirms earlier results (Gaskell 1982; Wilkes & Carswell 1982, Paper I).

(ii) O Iλ1304, C IIλ1335 are redshifted 1290, 1320 km s^{-1} respectively wrt the high-ionization lines and Lyα in high-redshift QSOs, larger than shifts reported previously.

(iii) The mean redshift of Lyα wrt C IV by $\sim$350 km s^{-1} in this sample is believed to be due to the combined effect of blending with N V in the red wing and Lyα forest absorption lines in the blue.

(iv) The dependence of the C III] line position upon redshift (Wills 1980) was not confirmed in this much smaller sample.

(v) The FWHM distribution of C III] has a larger mean and standard deviation than those of uncontaminated emission lines; this is consistent with the presence of blended features.

(vi) The mean effective wavelength for the 1400 Å feature is consistent with previous results and implies a ratio I(O IV])/I(Si IV) of 2.

(vii) The mean position of the O VIλ1034 feature implies contamination by Ly$\beta\lambda$1025 in a number of objects, confirming earlier reports (Paper I, Green *et al.* 1980).

Acknowledgments

I thank my collaborators in Australia: Drs A. E. Wright, D. L. Jauncey and B. A. Peterson for allowing me to further analyse the data presented in WWJP. I am greatly indebted to my thesis adviser, Dr R. F. Carswell for his continual help and guidance during the course of this research, to Drs R. J. Rudy and D. M. Whittle for enlightening discussion and the referee for his attention to detail. I also thank Linda Forbes and Helen Bluestein for their typing expertise. It is a pleasure

to thank the Director and staff of Steward Observatory for their hospitality during my stay there and to acknowledge the UK Science and Engineering Research Council for financial support on a NATO postdoctoral research fellowship.

References

Baldwin, J. A., 1975. *Astrophys. J.*, **201,** 26.
Baldwin, J. A., 1979. In: *Active Galactic Nuclei*, p. 51, ed. Hazard, C. & Mitton, S., Cambridge University Press.
Baldwin, J. A., Burbidge, E. M., Hazard, C., Murdoch, H. S., Robinson, L. B. & Wampler, E. J., 1973. *Astrophys. J.*, **185,** 739.
Baldwin, J. A., Wampler, E. J. & Burbidge, E. M., 1976. *Astrophys. J.*, **243,** 76.
Blumenthal, G. R. & Mathews, W. G., 1975. *Astrophys. J.*, **198,** 517.
Blumenthal, G. R. & Mathews, W. G., 1979. *Astrophys. J.*, **233,** 479.
Bolton, J. G., Peterson, B. A., Wills, B. J. & Wills, D., 1976. *Astrophys. J.*, **210,** L1.
Bromander, J., 1969. *Arkiv Fysik*, **40,** 257.
Browne, I. W. A. & Savage, A., 1977. *Mon. Not. R. astr. Soc.*, **177,** 77P.
Browne, I. W. A., Savage, A. & Bolton, J. G., 1975. *Mon. Not. R. astr. Soc.*, **173,** 87P.
Davidson, K. & Netzer, H., 1979. *Rev. Mod. Phys.*, **51,** 715.
Dumont, A. M. & Mathez, G., 1981. *Astr. Astrophys.*, **102,** 1.
Gaskell, C. M., 1981. *PhD thesis*, University of California, Santa Cruz.
Gaskell, C. M., 1982. *Astrophys. J.*, **263,** 79.
Gaskell, C. M., Shields, G. A. & Wampler, E. J., 1981. *Astrophys. J.*, **249,** 443.
Green, R. F., Pier, J. R., Schmidt, M., Estabrook, F. B., Lane, A. L. & Wahlquist, H. D., 1980. *Astrophys. J.*, **239,** 483.
Heckman, T. M., Miley, G. K., van Breugel, W. J. M. & Butcher, H. R., 1981. *Astrophys. J.*, **156,** 49.
Hewitt, A. & Burbidge, G. R., 1980. *Astrophys. J. Suppl.*, **43,** 57.
Jauncey, D. L., Batty, M. J., Wright, A. E., Peterson, B. A. & Savage, A., 1984. *Astrophys. J.*, **286,** 498.
Jauncey, D. L., Wright, A. E., Peterson, B. A. & Condon, J. J., 1978a. *Astrophys. J.*, **219,** L1.
Jauncey, D. L., Wright, A. E., Peterson, B. A. & Condon, J. J., 1978b. *Astrophys. J.*, **223,** L1.
Jauncey, D. L., Batty, M. J., Wright, A. E., Peterson, B. A. & Savage, A., 1984. *Astrophys. J.*, **286,** 498.
Jordan, C., 1969. *Astrophys. J.*, **156,** 49.
Krolik, J. H. & London, R. A., 1983. *Astrophys. J.*, **267,** 18.
Kwan, J. & Carroll, T. J., 1982. *Astrophys. J.*, **261,** 25.
Kwan, J. & Krolik, J. H., 1981. *Astrophys. J.*, **250,** 478.
Lynds, C. R., Stockton, A. N. & Livingstone, W. C., 1965. *Astrophys. J.*, **142,** 1667.
Mathews, W. G., 1974. *Astrophys. J.*, **189,** 23.
Netzer, H., 1976. *Mon. Not. R. astr. Soc.*, **177,** 473.
Osmer, P. & Smith, M. G., 1980. *Astrophys. J. Suppl.*, **42,** 523.
Osterbrock, D. E., 1977. *Astrophys. J.*, **215,** 733.
Osterbrock, D. E., Koski, A. T. & Phillips, M. M., 1976. *Astrophys. J.*, **206,** 898.
Peacock, J. A. & Wall, J. V., 1981. *Mon. Not. R. astr. Soc.*, **194,** 331.
Peterson, B. A., Jauncey, D. L., Wright, A. E. & Condon, J. J., 1976. *Astrophys. J.*, **207,** L5.
Peterson, B. A., Jauncey, D. L., Wright, A. E. & Condon, J. J., 1978. *Astrophys. J.*, **222,** L81.
Peterson, B. A., Wright, A. E., Jauncey, D. L. & Condon, J. J., 1979. *Astrophys. J.*, **232,** 400.
Savage, A., Bolton, J. G., Tritton, K. P. & Peterson, B. A., 1978. *Mon. Not. R. astr. Soc.*, **183,** 473.
Savage, A. & Wright, A. E., 1981. *Mon. Not. R. astr. Soc.*, **196,** 927.
Smith, H. E., Burbidge, E. M., Baldwin, J. A., Tohline, J. G., Wampler, G. J., Hazard, C. & Murdoch, H. S., 1977. *Astrophys. J.*, **215,** 427.
Smith, M. G., 1982. In: *Investigating the Universe*, p. 151, ed. Kahn, F. D., Reidel, Dordrecht, Holland.
Véron-Cetty, M.-P. & Véron, P., 1984. *ESO Sci. Rep. No. 1.*
Whelan, J. A. J., Smith, M. G. & Carswell, R. F., 1979. *Mon. Not. R. astr. Soc.*, **189,** 363.
Wilkes, B. J., 1984. (Paper I), *Mon. Not. R. astr. Soc.*, **207,** 73.
Wilkes, B. J. & Carswell, R. F., 1982. *Mon. Not. R. astr. Soc.*, **201,** 645.
Wilkes, B. J., Wright, A. E., Jauncey, D. L. & Peterson, B. A., 1983. (WWJP), *Astr. Soc. Aust. Conf. Proc.*, **5,** 2.
Wills, B. J., Netzer, H. & Wills, D., 1980. *Astrophys. J.*, **242,** 11.
Wills, D., 1980. *Astrophys. J.*, **240,** 721.
Wills, D. & Lynds, R., 1978. *Astrophys. J. Suppl.*, **36,** 317.

Wills, D. & Netzer, H., 1979. *Astrophys. J.,* **233,** 1.
Wills, D. & Wills, B. J., 1976. *Astrophys. J. Suppl.,* **31,** 143.
Wright, A. E., Ables, J. G. & Allen, D. A., 1983. *Mon. Not. R. astr. Soc.,* **205,** 793.
Wright, A. E., Jauncey, D. L., Peterson, B. A. & Condon, J. J., 1977. *Astrophys. J.,* **211,** L115.
Wright, A. E., Jauncey, D. L., Peterson, B. A. & Condon, J. J., 1978. *Astrophys. J.,* **226,** L61.
Wright, A. E., Morton, D. C., Peterson, B. A. & Jauncey, D. L., 1979a. *Mon. Not. R. astr. Soc.,* **189,** 611.
Wright, A. E., Peterson, B. A. & Jauncey, D. L., 1979b. *Mon. Not. R. astr. Soc.,* **188,** 711.
Wright, A. E., Peterson, B. A., Jauncey, D. L. & Condon, J. J., 1979c. *Astrophys. J.,* **229,** 73.
Young, P. J., Sargent, W. L. W. & Boksenberg, A., 1982. *Astrophys. J. Suppl.,* **48,** 455.